JOURNAL OF THERMOPHYSICS AND HEAT TRANSFER
Vol. 20, No. 4, October–December 2006

Model for Ammonia Solar Thermal Thruster

Gianpiero Colonna,* Giulia Capitta,† and Mario Capitelli‡
Università di Bari and Consiglio Nazionala delle Ricerche, Istituto di Metodologie Inorganiche e dei Plasmi, 70126 Bari, Italy
Ingrid J. Wysong§
Edwards Air Force Base, California, 93524-7660
and
Fred G. Kennedy‖
Defense Advanced Research Projects Agency, Arlington, Virginia 22203

DOI: 10.2514/1.18380

This work is an attempt to investigate the nozzle expansion characteristics of a solar thruster that uses ammonia as the propellant. For this purpose we have developed a state-to-state kinetic model to study the dissociation of ammonia in a supersonic nozzle expansion. The properties of the thruster depend on the ammonia dissociation degree in the reservoir, which can be very far from equilibrium due to the very slow dissociation kinetics at the thruster working conditions (less than 2000 K). We have extended the calculation for higher temperatures (greater than 2500 K) where ammonia dissociation is higher. Because of the presence of some hydrogen atoms, non-Boltzmann distributions have been observed.

Nomenclature

A	=	nozzle section
C_p	=	constant pressure heat capacity
C_v	=	constant volume heat capacity
c	=	speed of light
E_a	=	reaction activation energy
e	=	electron charge
h	=	Plank constant
K_d	=	rate coefficient of the direct reaction
K_{eq}	=	equilibrium constant
K_r	=	rate coefficient of the reverse reaction
M	=	Mach number
P_0	=	reservoir pressure
R	=	universal gas constant
T_0	=	reservoir temperature
T_v	=	vibrational temperature
v	=	vibrational quantum number
α	=	C_v/R
α_D	=	ammonia dissociation degree
ε_v	=	vibrational level energy
γ	=	C_p/C_v
ω_e	=	first order spectroscopic constant to calculate vibrational level energies
$\omega_e x_e$	=	second order spectroscopic constant to calculate vibrational level energies
$\omega_e y_e$	=	third order spectroscopic constant to calculate vibrational level energies
$\omega_e z_e$	=	fourth order spectroscopic constant to calculate vibrational level energies

Presented as Paper 4943 at the 38th AIAA Thermophysics Conference, Toronto, Ontario, 6–9 June 2005; received 23 June 2005; revision received 14 September 2005; accepted for publication 14 September 2005.

*Ph.D., Senior Researcher, Dipartimento di Chimica; gianpiero.colonna@ba.imip.cnr.it. Member AIAA.
†Student, Dipartimento di Chimica; jucapi@libero.it.
‡Professor, Dipartimento di Chimica; mario.capitelli@ba.imip.cnr.it. Member AIAA.
§Ph.D., Chief, Air Force Research Laboratory, Propulsion Directorate Division, Space and Missile Propulsion Division, Aerophysics Branch; ingrid.wysong@edwards.af.mil. Associate Fellow AIAA.
‖Ph.D., Program Manager; fkennedy@darpa.mil. Senior Member AIAA.

I. Introduction

RECENTLY, solar thermal propulsion (STP) engines have been investigated as a promising technology to enhance microsatellite maneuverability and enable new missions [1–4]. Solar thermal propulsion takes advantage of concentrated sunlight, typically at concentration ratios of up to 10000:1, to raise a heat exchanger to temperatures of several thousands of degrees K. At the Surrey Space Centre [1,2] (SCC), a small scale STP engine has been designed to use ammonia as the propellant. The main advantage of ammonia is that it is a storable liquid with low molar mass and easy handling characteristics and does not exhibit the serious toxicity and flammability risks posed by hydrazine.

To achieve improved performances, the ammonia gas is heated to 2000–2500 K, which should result in dissociation to N_2 and H_2 molecules, doubling the particle density and decreasing the average molecular weight of the mixture. This improves rocket performance by raising specific impulse I_{sp}, which varies as the inverse square root of molecular weight. The problem is that the dissociation kinetics at temperatures of interest in the engine are very slow and therefore the complete dissociation of ammonia molecules may not occur.

In this paper we have developed a kinetic model for ammonia mixtures applied to the nozzle investigated at SSC [1,2]. It is worth noting that we have introduced state-to-state kinetics to verify the presence of nonequilibrium vibrational distributions during the nozzle expansion. We have also investigated the behaviors of the engine for higher reservoir temperatures (3000–5000 K) where the dissociation of ammonia is complete.

II. Model Description

A. Nozzle Geometry

The nozzle used in the thruster has a conic geometry of the dimensions (in mm) shown in Table 1. These data have been provided by SSC researchers. The converging nozzle is quite short and so we choose to include part of the reservoir in the calculation through a connecting cone of the dimensions (in mm) shown in Table 2.

The nozzle is shown in Fig. 1.

The fluid dynamic model of the nozzle flow is based on the almost one-dimensional Euler equations for a variable section duct. The

Table 1 Geometrical characteristics of the considered nozzle

Quantity	Value
Throat radius	0.35
Exit radius	2.0
Exit-throat distance	6.2
Inlet radius	1.0
Inlet-throat distance	1.2

Table 2 Geometrical characteristics of reservoir and connecting cone

Quantity	Value
Reservoir radius	11.25
Connecting cone length	2.0

Euler equations are solved, for the stationary state, together with the perfect gas equation of state and the mass continuity for each species including the reaction contributions. The numerical scheme adopted is described in [5].

B. Chemical Model

To build the chemical kinetic models, we need to select both the species that must be taken into account and their mutual reactions. In the initial demonstration laboratory experiments, the pressure ranges from 1 to 4 atm and the temperature is less than 1500 K. For operational versions, the temperature could reach the value of 2500 K. The pressure values are measured directly, but the gas temperature is estimated from some measurements performed outside the reservoir. This results in a large uncertainty on the actual conditions operating inside the reservoir. For these temperatures the ammonia decomposition kinetics are quite slow. Surface dissociation, neglected in this approach, should probably be inserted in the model.

1. Species

We assume that the ammonia mixture consists of atoms and molecules formed in the NH_3 decomposition. We ignore all the ions because the temperatures involved are quite low. We introduce the vibrational excitation only for N_2 and H_2 molecules, which have stable vibrational excited levels. For all the other molecules, we disregard the internal levels as their number is so high that the computational load becomes unaffordable. Moreover, there is a lack of data for implementing state-to-state kinetics for NH_x molecules. A multitemperature model could be a valid approach assuring an acceptable computational cost nevertheless, in this work, we consider these internal states in equilibrium with the translational degree of freedom or as following a frozen kinetics, simulating nonequilibrium expansion. According to the internal state model selected we assign the C_p and $\gamma(\gamma = C_p/C_v)$ coefficients to each molecule. For each vibrational mode or rotational axis, in equilibrium with the translational degree of freedom, we add the quantity αR into the expressions of C_p and C_v, where the α parameter is set to 1 for a vibrational mode and 1/2 for a rotational axis. This approximation is valid for the rigid rotor and for the infinite harmonic oscillator, because in general the C_p coefficient depends on the temperature. For atomic species no internal degree of freedom is considered. The contribution of translational degrees to the molar specific heat is 2.5 R. Table 3 reports the species accounted and their relative properties. Rot is the number of independent rotational axes, Vib is the number of vibrational modes, and E_f is the formation energy.

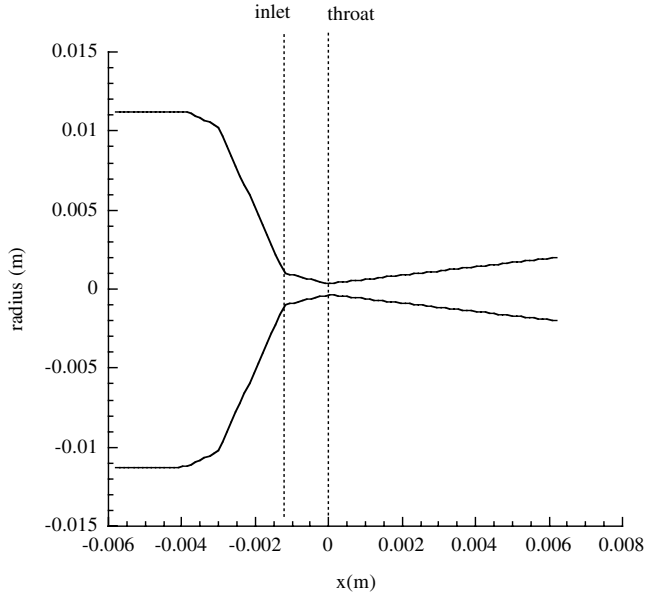

Fig. 1 Nozzle profile.

Table 3 Species inserted and their physical properties [6–11].

Species	Mass (AMU)	Rot	Vib	E_f (eV)
NH_3	17	3	6	−0.403242
N_2H_3	31	3	9	4.30994
NH_2	16	3	3	2.00285
NH	15	2	1	3.90225
N_2	28	2	1	0.00000
H_2	2	2	1	0.00000
N	14	0	0	4.87950
H	1	0	0	2.23910

For H_2 and N_2 we estimate the energy of each vibrational level (ε_v) through the semiempirical formula [12], function of the vibrational quantum number, and of some spectroscopic constants expressed in cm^{-1}:

$$\varepsilon_v = hc/e\{\omega_e[v + (1/2)] - \omega_e x_e[v + (1/2)]^2 + \omega_e y_e[v + (1/2)]^3 + \omega_e z_e[v + (1/2)]^4\} \quad (1)$$

The H_2 spectroscopic constants have been obtained through the fits of the vibrational level energies extracted from the Boothroyd, Keogh, Martin, and Peterson (BKMP) potential energy surface [13], whereas for N_2 we used data from [6]. Table 4 summarizes those values for the two species.

2. Processes

We implement in our model macroscopic kinetics for NH_3 depletion based on the following processes:

$$NH_3 + X \leftrightarrow NH_2 + H + X \quad (2a)$$

$$NH_3 + X \leftrightarrow NH + H_2 + X \quad (2b)$$

$$NH_3 + H \leftrightarrow NH_2 + H_2 \quad (2c)$$

$$NH + H + X \leftrightarrow NH_2 + X \quad (2d)$$

$$H_2 + N + X \leftrightarrow NH_2 + X \quad (2e)$$

$$NH_2 + H \leftrightarrow NH + H_2 \quad (2f)$$

$$NH_2 + NH_2 \leftrightarrow NH_3 + NH \quad (2g)$$

$$N + H + X \leftrightarrow NH + X \quad (2h)$$

$$NH + H \leftrightarrow H_2 + N \quad (2i)$$

Table 4 Constants (cm^{-1}) used to calculate vibrational energy [6] [see Eq. (1)].

Parameters	N_2	H_2
ω_e	2358.57	4464.7
$\omega_e x_e$	14.324	146.93
$\omega_e y_e$	−0.00226	4.7108
$\omega_e z_e$	0.0	−0.22712
E_{diss}	9.7639	4.4772
$V_{\max}$	48	15

$$NH + N \leftrightarrow N_2 + H \quad (2j)$$

$$NH + NH \leftrightarrow H_2 + N_2 \quad (2k)$$

$$2H + N_2 \leftrightarrow H_2 + N_2 \quad (2l)$$

$$2H + H_2 \leftrightarrow H_2 + H_2 \quad (2m)$$

$$2N + N_2 \leftrightarrow N_2 + N_2 \quad (2n)$$

$$2N + N \leftrightarrow N_2 + N \quad (2o)$$

$$NH_3 + NH_2 \leftrightarrow N_2H_3 + H_2 \quad (2p)$$

$$N_2H_3 + X \leftrightarrow NH_2 + NH + X \quad (2q)$$

$$N_2H_3 + H \leftrightarrow 2NH_2 \quad (2r)$$

$$N_2H_3 + H \leftrightarrow NH_3 + NH \quad (2s)$$

where X is a generic component. The rate coefficients for all these processes are expressed in the Arrhenius form [12]:

$$K = K_0 T^{\delta} e^{-E_a/T} \quad (3)$$

For the direct reaction, the parameters K_0, δ, and E_a are reported in Table 5. K_0 has the dimension of $cm^{3(n-1)}/s$, where n is the number of particles involved in the reaction, E_a is expressed in K, and δ is a dimensionless parameter [Eq. (3)]. The rate coefficients of these processes have been taken from [6–11]. In this model, we neglect more complex molecules, such as N_2H_4, that do not seem to be significant.

Rates for the reverse processes have been obtained through the detailed balance principle [12]:

$$K_r = K_d / K_{\text{eq}} \quad (4)$$

Equilibrium constants have been calculated from partition functions, following the classical statistical thermodynamic theory [14]. Subsequently they have been fitted by the equation

$$\ell_n(K_{\text{eq}}) = K_\infty + K_p(1000/T)^{q_p} + K_e e^{-T/q_e} \quad (5)$$

We consider only the equilibrium constants for the generation of a new species from standard ones like N_2 and H_2 in nitrogen-hydrogen compounds formation. Therefore all the formation reactions can be synthesized as

$$(n/2)N_2 + (m/2)H_2 \leftrightarrow N_nH_m \quad (6)$$

The parameter values used to calculate K_{eq}, for the species listed in Table 3, are reported in Table 6. From these formation equilibrium constants we can calculate the equilibrium constants relative to all the reactions involving the species in the table.

Table 5 Arrhenius coefficients for the reactions inserted in the model [6–11].

Process	K_0	δ	E_a	Reference
(2a)	$1.53e-8$	0	42,400	9
(2b)	$1.00e-9$	0	47,000	9
(2c)	$3.20e-13$	0.67	1720	9
(2d)	$1.00e-32$	0	0	13
(2e)	$1.00e-34$	0	0	12
(2f)	$2.30e-13$	0.67	2160	13
(2g)	$6.64e-12$	0	2800	13
(2h)	$1.00e-33$	0	0	13
(2i)	$1.70e-12$	0.68	957	12
(2j)	$1.77e-11$	0	0	12
(2k)	$6.60e-13$	0.55	957	10
(2l)	$1.34e-31$	−0.60	0	0
(2m)	$2.68e-31$	−0.60	0	10
(2n)	$7.44e-32$	−0.50	0	10
(2o)	$3.31e-27$	−1.50	0	8
(2p)	$1.33e-12$	0.5	0	8
(2q)	$1.70e-8$	0.	21,000	8
(2r)	$2.60e-12$	0	0	8
(2s)	$1.70e-13$	0	0	8

Table 6 Coefficients of Eq. (5) for formation equilibrium constants. The pressures are in Pa.

Species	K_∞	K_p	q_p	K_e	q_e
NH_3	51.8293	−13.1631	0.960208	−7.97367	628.095
NH_2	19.6666	63.4542	1.01863	13.5452	311.287
NH	−5.14978	85.2911	0.998065	−2.21874	423.673
N	28.3772	−114.298	0.997620	−2.14877	4371.66
H	26.1506	−52.7759	0.996362	−2.71911	2157.34

The kinetic model has been improved including state-to-state kinetics for the diatomic species N_2 and H_2, substituting the processes (2l–2o) with the state-selective dissociation and adding vibrational relaxation processes [15–17].

$$N_2(v) + N_2(w) \leftrightarrow N_2(v-1) + N_2(w+1) \quad (7a)$$

$$N_2(v) + N_2(w) \leftrightarrow N_2(v-1) + N_2(w) \quad (7b)$$

$$N_2(v) + N \leftrightarrow N_2(v-\Delta v) + N \quad (7c)$$

$$N_2(v) + N_2(w) \leftrightarrow N_2(v-1) + 2N \quad (7e)$$

$$N_2(v) + N_2(w) \leftrightarrow 2N + N_2(w) \quad (7f)$$

$$N_2(v) + N \leftrightarrow 2N + N \quad (7g)$$

$$H_2(v) + H_2(w) \leftrightarrow H_2(v-1) + H_2(w+1) \quad (7h)$$

$$H_2(v) + H_2(w) \leftrightarrow H_2(v-1) + H_2(w) \quad (7i)$$

$$H_2(v) + H \leftrightarrow H_2(v-\Delta v) + H \quad (7j)$$

$$H_2(v) + H_2(w) \leftrightarrow H_2(v-1) + 2H \quad (7k)$$

$$H_2(v) + H_2(w) \leftrightarrow 2H + H_2(w) \quad (7l)$$

$$H_2(v) + H \leftrightarrow 2H + H \quad (7m)$$

All the other processes involve only the ground state of such molecules. We have also included vibrational relaxation of nitrogen molecules due to hydrogen [6,9]:

$$N_2(v) + H_2(w) \leftrightarrow N_2(v-1) + H_2(w) \tag{8a}$$

$$N_2(v) + H \leftrightarrow N_2(v-\Delta v) + H \tag{8b}$$

$$N_2(v) + H_2(w) \leftrightarrow N_2(v-1) + H_2(w+1) \tag{8c}$$

III. Results

A. Low Reservoir Temperature ($T < 2500$ K)

In this paragraph we want to investigate the kinetic behavior of the ammonia mixture in cases close to the working conditions of the solar thruster studied at the Surrey Space Centre [1,2]. The pressure range is between 1 and 4 bar and the temperature is less than 1500 K. The heater temperature is not well known because it has been measured [1,2] outside the chamber. We have extended our calculations to temperature values below 2500 K, which may be obtained in orbital conditions.

We investigate four different pressure values in the range 1–4 bar. In Fig. 2 we report the concentration profiles along the nozzle obtained for reservoir conditions of $P = 4$ bar and $T = 1500$ K, and introducing the vibrational kinetics of N_2 and H_2. It is interesting to observe that the flow is practically frozen along the whole nozzle except for some minor species such as H and NH_2 that completely disappear at the nozzle exit. The atomic nitrogen molar fraction is lower than 10^{-10}. Inspection of Fig. 1 shows that the contribution of NH_x molecules to the flow characteristics is negligible because the concentration is very small.

Figures 3 and 4 describe the vibrational distributions of hydrogen and nitrogen for the conditions of Fig. 2. We can observe that the nitrogen distributions are frozen. On the contrary, although H_2 distributions for $v \leq 3$ are almost frozen, their tails are strongly depleted, resulting in non-Boltzmann distributions. The different behavior of the two species is due to the different percentage of nitrogen and hydrogen atoms; hydrogen atom concentration is high enough so that the VT collisions involving atoms are frequent enough to cool the distribution tails.

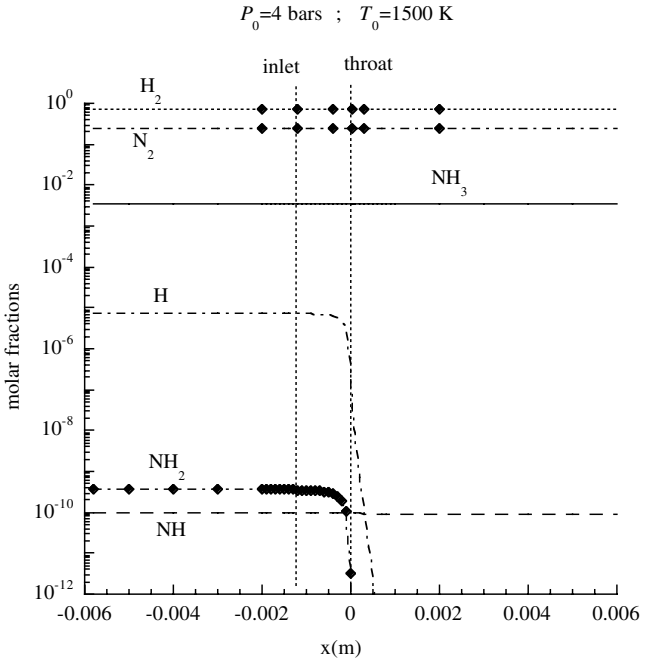

Fig. 2 Molar fractions of mixture species along the nozzle. We assume as reservoir conditions $P_0 = 4$ bars and $T_0 = 1500$ K and starting from an equilibrium inlet composition.

The distribution behavior brings two conclusions: first of all the contribution of vibrational kinetics is practically negligible and the vibrational temperature can be considered frozen, at least for diatomic molecules. As a consequence, in the following results we have used only the macroscopic model freezing the vibrational temperature of all the molecules, in the sense that the contribution of the vibrational degrees of freedom is null. This results in neglecting the vibrational contribution ("Vib" in Table 3) in the calculation of C_p.

We observe that the M is practically independent of the initial temperature and pressure, obtaining at the nozzle exit a value close to $M = 5.4$. We report the pressure along the nozzle in Fig. 5. It is quite interesting to note that the exit pressure is proportional to the inlet pressure. These two results occur as the chemistry weakly affects the macroscopic quantities during the expansion.

Table 7 reports the mass flow rate and the thrust for different inlet pressures at $T_0 = 1500$ K except when marked with the * symbol assigned to $T_0 = 2500$ K. At the inlet we suppose an equilibrium composition. Table 8 on the other hand, reports experimental results of mass flow rate and thrust measured on the solar microcavity receiver MKI by Kennedy et al. [1]and Kennedy and Palmer [2].

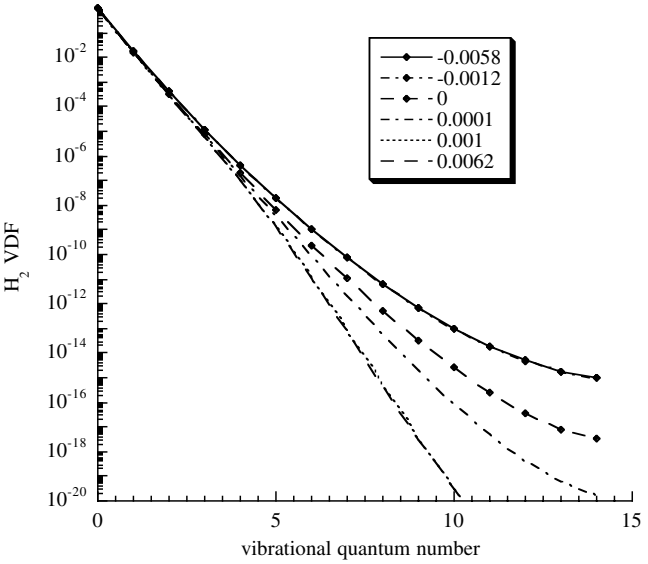

Fig. 3 Hydrogen vibrational distributions at different nozzle positions (in meters) in the same conditions as in Fig. 2.

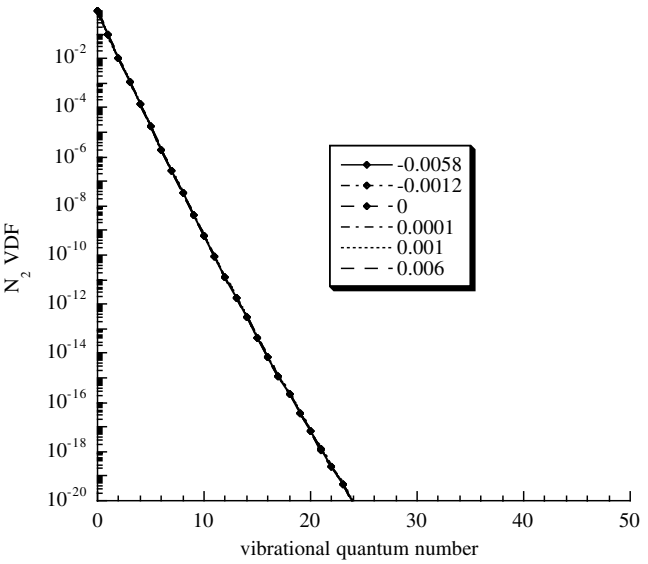

Fig. 4 Nitrogen vibrational distributions at different nozzle positions (in meters) in the same conditions as in Fig. 2.

Table 7 Computed mass flow rate and thrust of the nozzle as a function of the inlet pressure.

P_o (bar)	Mass flow rate (g/s)	Thrust (mN)
1	$2.1374e-2$	63.379
2	$4.2766e-2$	126.71
3	$6.4122e-2$	189.99
4	$8.5496e-2$	253.58
4*	$6.6917e-2$	256.05

Table 8 Experimental values for different test cases.

Mass flow rate (g/s)	Thrust (mN)
.140	219
.147	223
.117	183
.121	190

Chamber pressure varies in the range of 2.5–4 bar while a temperature of about 1500 K was estimated. Comparison of the experimental results with the theoretical ones shows: 1) the theoretical mass flow rates are lower than the experimental ones; and 2) the theoretical and experimental thrust values are in the same range. This point will be discussed at the end of this section.

In this temperature range the kinetics of ammonia presents large uncertainties [6–11], even though it has been widely studied. The main problem is that the slow kinetics prevents us from estimating the kinetic constants precisely. Experimental works [1,2] on ammonia thrusters assume a complete decomposition of ammonia in the reservoir, but the kinetic scheme proposed does not lead to equilibrium conditions in an acceptable time for $T < 2000$ K. Under these conditions the most important problem is that it is possible that in the inlet conditions there is not chemical equilibrium as usually happens in nozzle reservoirs. Because of this, we also try as an initial condition a pure ammonia gas.

Dissociation inside the reservoir and the nozzle is very poor, so that again in this case the flow is frozen. As a consequence, the flow properties depend only on the C_p/C_v ratio and on the mean molar mass, and so the exit properties are completely different from the equilibrium case. As an example in Fig. 6 we compare the M computed starting from an equilibrium composition and from pure ammonia (nonequilibrium). It is not possible to really know what composition prevails inside the reservoir for $T < 2000$ K, moreover some impurities or wall catalytic effects can accelerate the kinetics, bringing the system to equilibrium faster than predicted by our kinetic model.

We try the same comparison at $T_0 = 2500$ K. In this case, the mixture reaches the equilibrium composition in the reservoir. Nevertheless, the M profiles in the equilibrium and nonequilibrium case are again different (see Fig. 7). This is the demonstration that the history of the gas in the reservoir is important.

Effects of initial conditions propagate also on the temperature profiles. In Fig. 8 we show the normalized temperature profile calculated starting from an equilibrium condition and from an undissociated ammonia (nonequilibrium) for a reservoir temperature of 1500 K and a pressure of 4 bar. We observe that the exit temperature is much higher in the case of the equilibrium conditions. This behavior could be due to the lower mean molar mass associated with the mixture in equilibrium composition inside the reservoir.

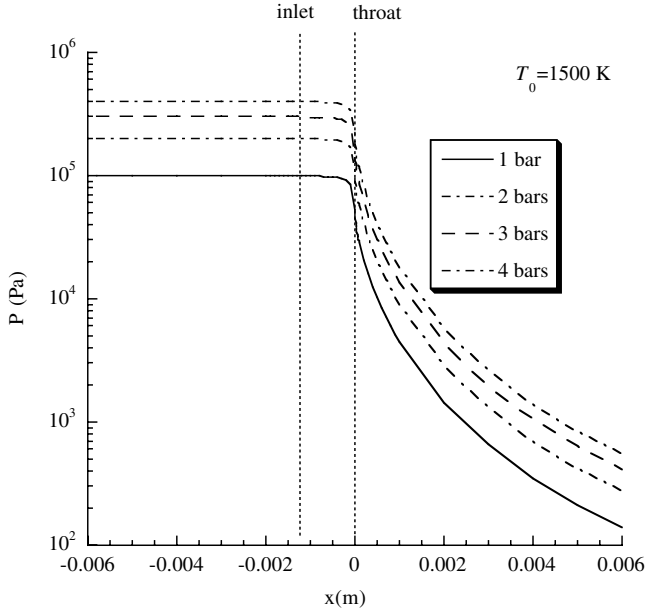

Fig. 5 Pressure profile along the nozzle as a function of the inlet pressure for $T_0 = 1500$ K and starting from an inlet equilibrium composition.

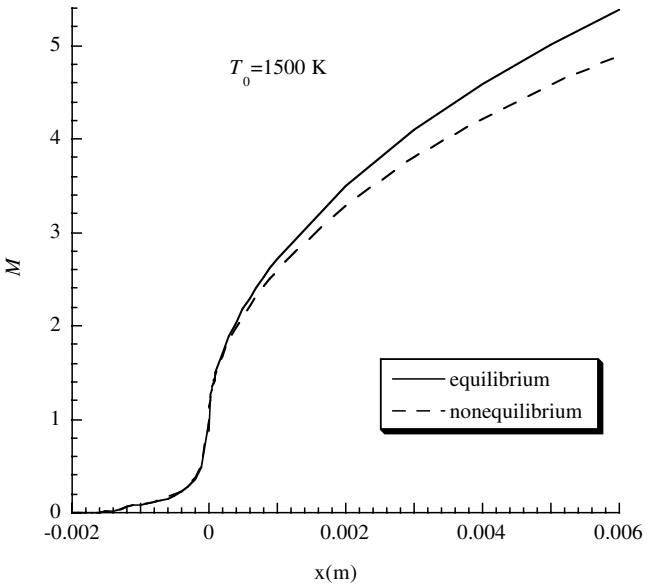

Fig. 6 M profile compared for inlet equilibrium and pure ammonia (nonequilibrium) case (pressure and temperature conditions as in Fig. 2).

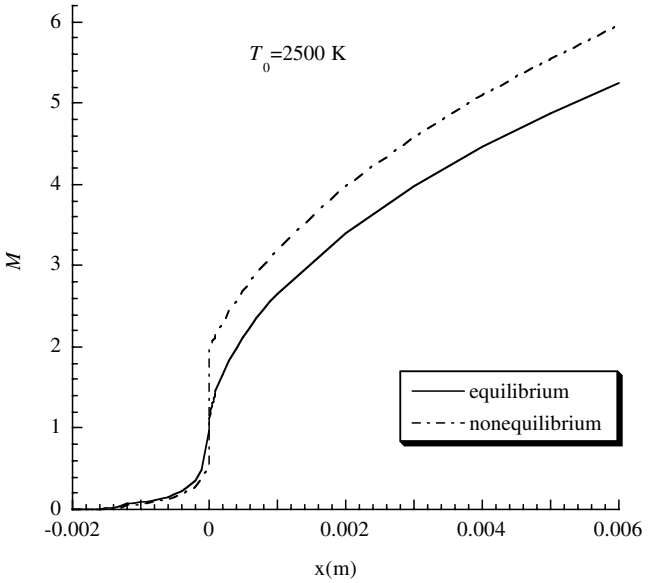

Fig. 7 Same as in Fig. 6 with reservoir temperature $T_0 = 2500$ K and pressure $P_0 = 4$ bars.

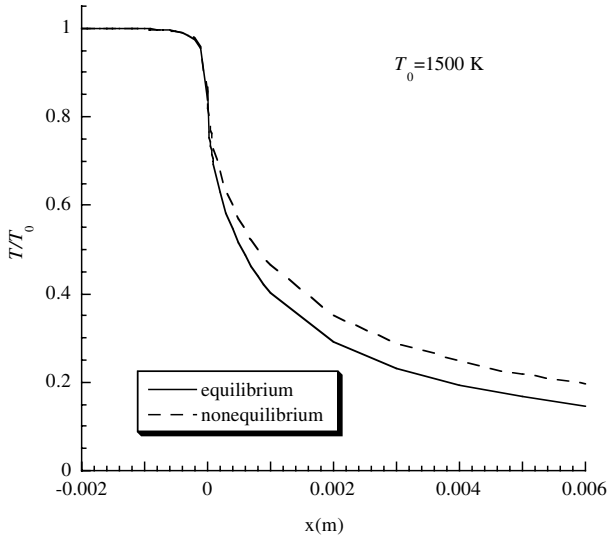

Fig. 8 Reduced temperature profile compared for inlet equilibrium or pure ammonia (nonequilibrium) case (pressure and temperature conditions as in Fig. 2).

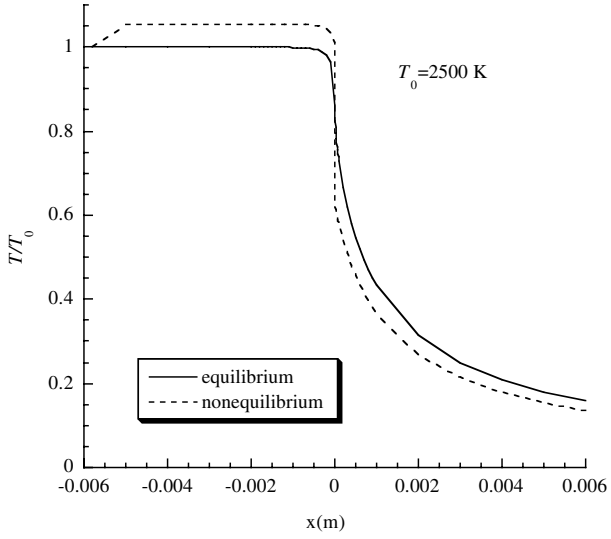

Fig. 9 Reduced temperature profile compared for inlet equilibrium or pure ammonia (nonequilibrium) case, for a reservoir temperature $T_0 = 2500$ K and pressure $P_0 = 4$ bars.

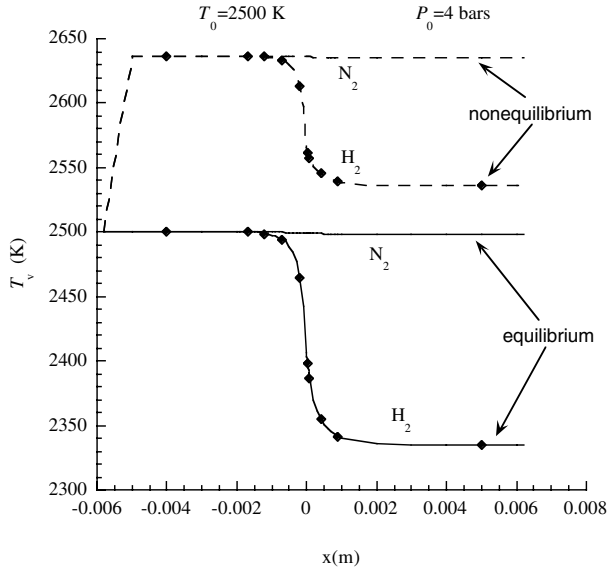

Fig. 10 Vibrational temperature profile of N_2 and H_2 in the same conditions as in Fig. 9.

Table 9 Theoretical quantities as a function of α_D for frozen vibration. $P_0 = 4$ bar, $T_0 = 1500$ K.

α_D	Mass flow rate (g/s)	Thrust (mN)	I_{sp}
0.0	$1.2120e-1$	261.56	220
0.2	$1.1099e-1$	260.72	239
0.4	$1.0317e-1$	259.64	256
0.8	$9.1461e-2$	257.96	287
1.0	$8.5496e-2$	253.52	302

Different behaviors occur when the reservoir temperature reaches 2500 K (see Fig. 9). In fact, at this temperature, the reactions in the inlet are faster than in the flow, therefore one can observe an increase of the temperature due to the mixture dissociation. Even if the ammonia energy is lower than that of nitrogen and hydrogen molecules, the compression due to the double particle number density produces an increase of the temperature. At the nozzle exit, the differences are lower than in the case of an inlet temperature of 1500 K.

For $T_0 = 2500$ K, vibrational kinetics can have appreciable effects, therefore, we perform our calculation including the vibrational levels. We find similar behaviors for the relaxation of the vibrational temperature, calculated as the temperature of the first excited level (Fig. 10). Starting from nonequilibrium conditions, we can observe an increase of the vibrational temperatures following the gas temperature. At the nozzle exit, the vibrational temperature freezes at a temperature higher than 2300 K just after the throat. N_2 vibrational temperature is practically frozen.

As a consequence of the previous results, we can state that there are some uncertainties about the inlet composition. To demonstrate the sensitivity, we have reported in Table 9 the calculated mass flow rate and thrust for different dissociation degrees of ammonia for the process $NH_3 = 1.5H_2 + 0.5N_2$, defined as

$$\alpha_D = 1 - \frac{[NH_3]}{[NH_3] + .5[N_2]}$$

that ranges from 0 (pure ammonia) to 1 (N_2 and H_2 mixture). We note that both quantities decrease when the dissociation degree increases, but the thrust changes more slowly than the mass flow rate, and so the specific impulse will be higher for the dissociated case. Inlet pressure and temperature are $P_0 = 4$ bar and $T_0 = 1500$ K. Vibrational degrees of freedom are frozen.

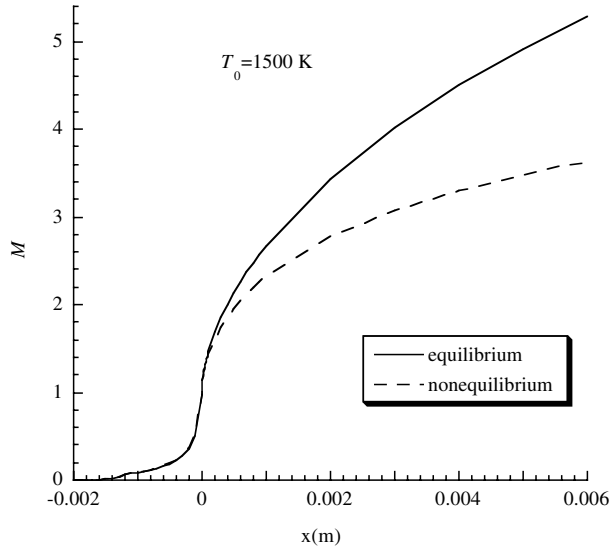

Fig. 11 M profile compared for inlet equilibrium and pure ammonia (nonequilibrium) case (pressure and temperature conditions as in Fig. 2). The vibrational degrees of freedom are in equilibrium with the translational ones.

Table 10 Theoretical quantities as a function of α_D for equilibrium vibration. $P_0 = 4$ bar, $T_0 = 1500$ K.

α_D	Mass flow rate (g/s)	Thrust (mN)	I_{sp}
0.0	$1.1364e-1$	282.55	253
0.2	$1.0438e-1$	282.42	274
0.4	$9.7589e-2$	276.91	289
0.8	$8.7962e-2$	269.78	312
1.0	$8.2806e-2$	261.59	322

The last aspect that needs to be investigated is the role of internal degrees of freedom, in particular molecular vibration, to the measured quantities (thrust and mass flow rate). The main problem is that nothing is known about vibrational relaxation of ammonia molecules. Therefore, we compare the results obtained with a frozen vibrational kinetics with those obtained considering the vibrational states in equilibrium with the translational degrees of freedom (see Fig. 11 and Table 10). Inlet pressure and temperature are $P_0 = 4$ bar and $T_0 = 1500$ K. Vibrational degrees of freedom are in equilibrium with the translational ones. It can be observed that the mass flow rate and the specific impulse are weakly affected by the internal state kinetics even if some macroscopic quantities such as M are strongly influenced by the vibrational contribution, especially when the inlet ammonia concentration is high. This is due to the large number of vibrational modes of ammonia molecules.

It should be noted that the new theoretical results with undissociated ammonia ($a_d \sim 0$) are in better agreement with the experimental mass flow rates even though the comparison with thrust values is a little worse. More detailed experimental data are in any case necessary to validate the present model, which, however, at this stage of development represents a useful tool for predicting the performances of ammonia solar thrusters. It is also noted that [1] points out evidence of receiver leakage around the seals during the measurements, which may account for the surprisingly low measured thrust values. However, the simulation results presented here provide a strong indication that the ammonia propellant is in fact far from completely dissociated under these conditions.

B. High Reservoir Temperature ($T > 2500$ K)

In the previous section we studied the behavior of the ammonia solar thruster in the working conditions of the thruster investigated experimentally in [1,2]. In this section we want to understand the behavior of the expansion for higher temperature ranges (3000 K $\leq T_0 \leq$ 5000 K). For temperature $T_0 > 2500$ the ammonia dissociation is very fast.

Moreover in the considered temperature range the molar fraction of atomic hydrogen is not negligible. For this condition, due to the recombination of hydrogen atoms and to atom-molecule vibration-translation collisions, nonequilibrium vibrational distributions can be observed and non-Arrhenius chemical rates are obtained [15], inducing anomalous behavior in the kinetics.

Here we want to focus on the differences between the results obtained with two different models: 1) macroscopic kinetics, and 2) state-to-state kinetics.

In Fig. 12 we have compared the molar fractions of some species calculated with the two models. It is possible to observe that the H_2 molar fraction increases when the state-to-state model is considered, whereas the macroscopic model predicts a frozen concentration. In contrast, NH_2 and NH molar fractions show smaller variations when the state-to-state approach is used.

This behavior affects the macroscopic quantities such as the gas speed, the temperature, and the thrust. In Fig. 13 we have compared the axial speed profile in the two kinetic models at two different reservoir temperatures. There are appreciable differences at the nozzle exit especially for reservoir temperature $T_0 = 5000$ K. This effect is the consequence of the stronger recombination of hydrogen atoms producing H_2 molecules as can be observed in Fig. 12. Similar behaviors can be observed in the gas temperature profile (Fig. 14) and in the thrust (Fig. 15). An important result is that the calculated thrust

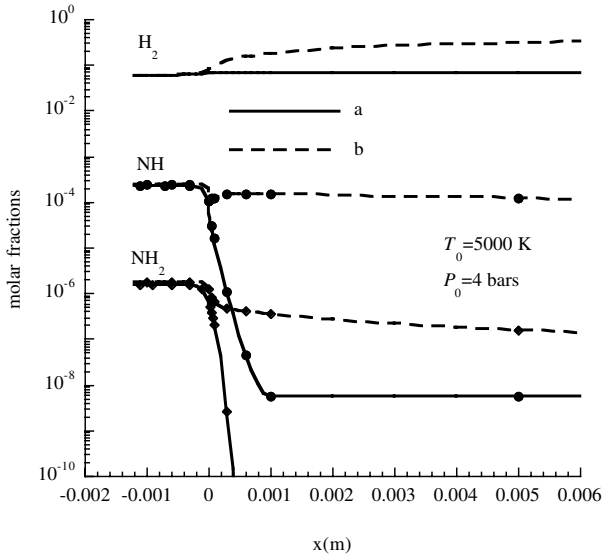

Fig. 12 Molar fraction profiles calculated with different kinetic models.

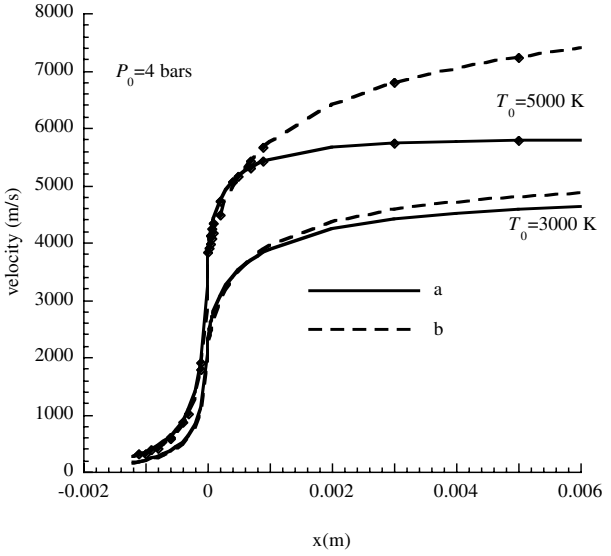

Fig. 13 Velocity profiles calculated with different kinetic models and inlet temperatures.

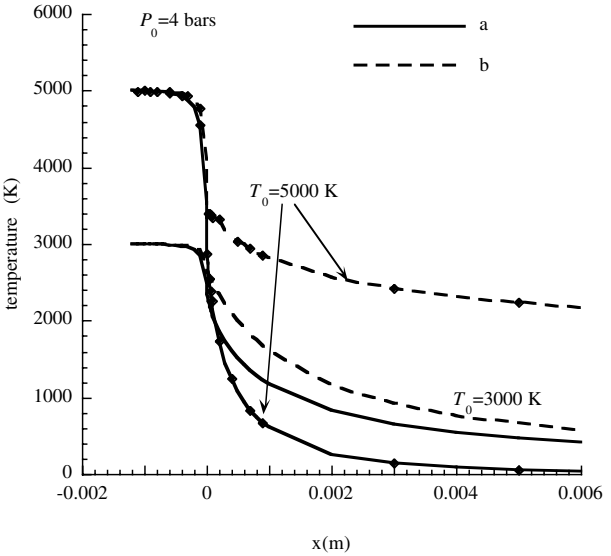

Fig. 14 Temperature profiles calculated with different kinetic models and inlet temperatures.

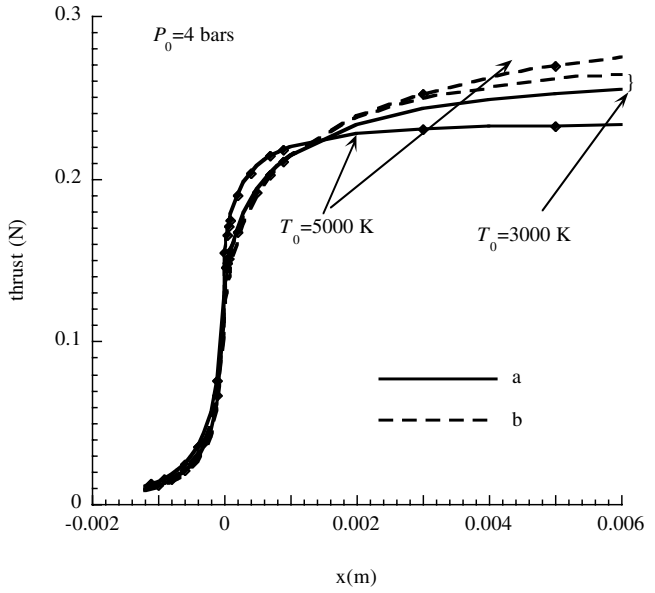

Fig. 15 Thrust profiles calculated with different kinetic models and inlet temperatures.

(and therefore the performance) is higher when the state-to-state vibrational kinetic model is included in the calculation.

As for the low temperature case, the molar fraction of NH_x species is small so that their influence to the flow properties is negligible. However, nonequilibrium vibrational distributions of such molecules could affect the gas composition due to deviations of the global rates from the Arrhenius trend.

IV. Conclusion

In this paper we have investigated the chemical kinetic aspects of an ammonia mixture for application to solar thermal thrusters. We have obtained results that contradict the common assumption of considering inlet conditions in equilibrium. If the kinetics of the mixture are very slow, as in the case of ammonia, the gas composition can be far from equilibrium. The comparison of measured mass flow rates with a range of assumed dissociation fractions also supports the conclusion that ammonia propellant at this temperature may be substantially undissociated. At low reservoir temperature ($T_0 <$ 2500 K), that is the working condition for the thruster in the laboratory, the kinetics of internal states is negligible, and the macroscopic and state-to-state models gives the same results, mainly because the flow is almost frozen. On the other end, at higher reservoir temperature ($T_0 \geq 3000$ K), when the hydrogen dissociation is important, the vibrational kinetics become very important. In these conditions the macroscopic and the state-to-state models predict different results, mainly due to the different atomic recombination.

We must emphasize that this study is preliminary. Some properties of the mixtures have been neglected, such as the vibrational kinetics of the NH_x molecules and the formation of NH molecules by vibrationally excited N_2 and H_2. The model can be improved including a multitemperature approach to account for the vibration of polyatomic molecules and by adding new state-to-state reactions between N_2 and H_2.

Acknowledgment

This work has been supported by the U.S. Air Force European Office of Aerospace Research and Development.

References

[1] Kennedy, F., Palmer, P., and Paul, M., "Microscale Solar Thermal Engine Ground Test Campaign at the Surrey Space Centre," AIAA, Paper_2004-4137, 2004.

[2] Kennedy, F., and Palmer, P., "A Comparison of Simulation and Test Campaign Results for a Microscale Solar Thermal Engine," *54th International Astronautical Congress*, International Astronautical Federation, Paris, 2003.

[3] Nakamura, T., Sullivan, D., McClanahan, J., Shoji, J., and Quinn, S., "Solar Thermal Propulsion for Small Spacecraft," AIAA, Paper_2004-4138, 2004.

[4] Baker, A. M., Curiel, A. D. S., and Schaffner, J., "'You Can Get There From Here': Advanced Low Cost Propulsion Concepts for Small Satellites Beyond LEO," *Acta Astronautica*, Vol. 57, No. 2-8, 2005, pp 288–301

[5] Colonna, G., Tuttafesta, M., and Giordano, D., "Numerical Methods to Solve Euler Equations in One-dimensional Steady Nozzle Flow," *Computer Physics Communications*, Vol. 138, No. 3, 2001, pp. 213–221.

[6] Capitelli, M., Ferreira, C. M., and Gordiets, B. F., *Plasma Kinetics in Atmospheric Gases*, Springer, Berlin, 2000.

[7] Starikovskaia, S. M., Starikovskii, A. Yu., and Zatsepin, D. V., "Hydrogen Oxidation in a Stoichiometric Hydrogen-Air Mixture in the Fast Ionization Wave," *Combustion Theory and Modelling*, Vol. 5, No. 1, 2001, pp. 97–129.

[8] Yasui, K., "Chemical Reactions in Sonoluminescing Bubble," *Journal of the Physical Society of Japan*, Vol. 66, 1997, pp. 2911–2920.

[9] Gordiets, B., Ferreira, C. M., Pinheiro, M. J., and Ricard, A., "Self Consistent Kinetic Model of Low Pressure N_2-H_2 Flowing Discharges: 1. Volume Processes," *Plasma Sources Science and Technology*, Vol. 7, No. 3, 1998, pp. 363–378.

[10] Yumura, M., Asaba, T., Matsumoto, Y. H., and Matsui, Y., "Thermal Decomposition of Ammonia," *Journal of Computational Chemistry*, Vol. 1, 1980, pp. 439–450.

[11] Davidson, D. F., Kohse-Höingaus, K., Chang, A. Y., and Hanson, R. K., "A Pyrolisis Mechanism for Ammonia," *International Journal of Chemical Kinetics*, Vol. 22, No. 5, 1990, pp. 513–535.

[12] Park, C., *Nonequilibrium Hypersonic Aerothermodynamics*, Wiley, New York, 1990.

[13] Boothroyd, A. I., Keogh, W. J., Martin, P. G., and Peterson, M. R., "A Refined H_3 Potential Energy Surface," *Journal of Chemical Physics*, Vol. 104, No. 18, 1996, pp. 7139–7169.

[14] Landau, L. D., *Statistical Physic*, Elsevier, Amsterdam, 1979.

[15] Colonna, G., Tuttafesta, M., Capitelli, M., and Giordano, D., "Non-Arrhenius NO Formation Rates in One-Dimensional Nozzle Airflow," *Journal of Thermophysics and Heat Transfer*, Vol. 13, No 3, 1999, pp. 372–375.

[16] Capitelli, M., Colonna, G., and Esposito, F., "On the Coupling of Vibrational Relaxation with the Dissociation-Recombination Kinetics: From Dynamics to Aerospace Applications," *Journal of Physical Chemistry A*, Vol. 108, No. 41, 2004, pp. 8930–8934.

[17] Colonna, G., Esposito, F., and Capitelli, M., "H_2 State to State Kinetics in Nozzle Expansion," American Inst. of Physics, No. 762, 2005.